

# Fast-Light Enhanced Brillouin Laser Based Active Fiber Optic Sensor for Simultaneous Measurement of Rotation and Strain

Minchuan Zhou, Zifan Zhou, Mohamed Fouda, Nicholas Condon, Jacob Scheuer, *Senior Member, IEEE*, and Selim M. Shahriar, *Member, IEEE*

**Abstract**—We have developed a conceptual design for an active fast light fiber optic sensor (AFLIFOS) that can perform simultaneously or separately as a gyroscope (differential mode effect) and as a sensor for strain and other common mode effects. Two Brillouin lasers in opposite directions and separated in frequency by several free spectral ranges are used for this sensor. By coupling two auxiliary resonators to the primary fiber resonator, we produce superluminal effects for the two laser modes. We develop a detailed theoretical model for optimizing the design of the AFLIFOS, and show that the enhancement factor of the sensitivity is  $\sim 8.2 \times 10^3$ , under the optimized condition, when the effective change in the length of the primary fiber resonator is 0.1 pm, corresponding to a rotation rate of  $1.4 \times 10^{-3}$  deg/sec. With this enhancement factor, the minimum detectable rotation rate is  $2.4 \times 10^{-11}$  deg/sec when the output power is 1 mW and the measurement time is 1 s, which is  $\sim 8.2 \times 10^3$  times better than that of the passive version with the same parameters. The minimum measurable strain is  $1.4 \times 10^{-2}$  fε/√Hz when 1/4 of the primary resonator is sensitive to strain and the linewidth of the master laser is taken to be 200 Hz. It may be possible to get much higher enhancement by adjusting parameters such as the length of the laser loops and the coupling coefficients.

**Index Terms**—Brillouin scattering, fast light, fiber optics, gyroscopes.

## I. INTRODUCTION

**O**PTICAL interferometers and resonators are commonly used for precision measurement. These devices can

Manuscript received February 28, 2017; revised September 22, 2017; accepted October 29, 2017. Date of publication October 31, 2017; date of current version November 20, 2017. This work was supported in part by the AFOSR under Grant FA9550-10-01-0228, in part by the NASA under Grants NNM13AA60C, NNX15CM35P, and NNX16CM03C, and in part by the Darpa under Grant W911NF-15-1-0643. (Corresponding Author: Minchuan Zhou.)

M. Zhou is with the Department of Physics, Northwestern University, Evanston, IL 60208 USA (e-mail: minchuanzhou2013@u.northwestern.edu).

Z. Zhou and M. Fouda are with the Department of Electrical Engineering and Computer Science, Northwestern University, Evanston, IL 60208 USA (e-mail: zifanzhou2012@u.northwestern.edu; mohamedfouda2015@u.northwestern.edu).

N. Condon is with the Department of Electrical Engineering and Computer Science, Northwestern University, Evanston, IL 60208 USA, and with the Digital Optics Technologies, Inc., Rolling Meadows, IL 60008 USA (e-mail: condon.optidot@gmail.com).

J. Scheuer is with the Department of Electrical Engineering, Tel Aviv University, Tel Aviv 69978, Israel (e-mail: kobys@eng.tau.ac.il).

S. M. Shahriar is with the Department of Electrical Engineering, and Computer Science and the Department of Physics, Northwestern University, Evanston, IL 60208 USA (e-mail: shahriar@northwestern.edu).

Color versions of one or more of the figures in this paper are available online at <http://ieeexplore.ieee.org>.

Digital Object Identifier 10.1109/JLT.2017.2768898

accurately measure the phase shifts of light due to rotation and strain. It is shown in Ref. 1, that the coupled resonant optical waveguide (CROW) gyroscopes do not offer any fundamental enhancement in the sensitivity of rotation measurement. Recently, much theoretical and experimental work [1]–[16] has been carried out for enhancing the sensitivity of such devices using the superluminal effect, which produces a very small group index that is inversely proportional to the sensitivity. These studies considered both passive [1]–[8], [10], [11], [13]–[15] and active [2]–[7], [9], [10], [12] versions of the resonators. Furthermore, different physical mechanisms have been considered, in both active and passive cases, for realizing the anomalous dispersion that produces the superluminal effect. Previously, we have shown that in a passive resonator, the enhancement from the superluminal effect is practically eliminated by the concomitant broadening of the resonator linewidth [6]. Such an offset is circumvented in an active resonator, where the dispersive cavity contains an active gain medium [6]. In this paper, we consider the case of an active resonator, for which the superluminal effect is produced via coupling to other resonators [17]. Specifically, we describe a system called Active Fast Light Fiber Optic Sensor (AFLIFOS). It consists of a primary fiber resonator that is coupled to two auxiliary resonators for creating the superluminal effects for two counter-propagating Brillouin laser modes.

The rest of the paper is organized as follows. In Section II, we introduce the realization of the fast light effect using additional cavity resonators. In Section III, we describe the scheme of the AFLIFOS. In Section IV, we theoretically model the AFLIFOS and show the results of the sensitivity enhancement factor under optimized condition. In Section V, we describe the design for stabilizing the perimeters of the cavity resonators using master lasers. In Section VI, we discuss the detection process for common-mode and differential-mode effects. We conclude in Section VII with a summary of our results and future plans.

## II. CAVITY PHASE ELEMENT

The basic concept of the AFLIFOS is schematically illustrated in Fig. 1(a). Two non-degenerate pump beams (P1 and P2) are sent into a fiber resonator and two counter-propagating Brillouin lasers (B1 and B2) are generated opposite to the propagating directions of the respective pump beams. Two additional rings are coupled to the primary ring resonator in order to produce

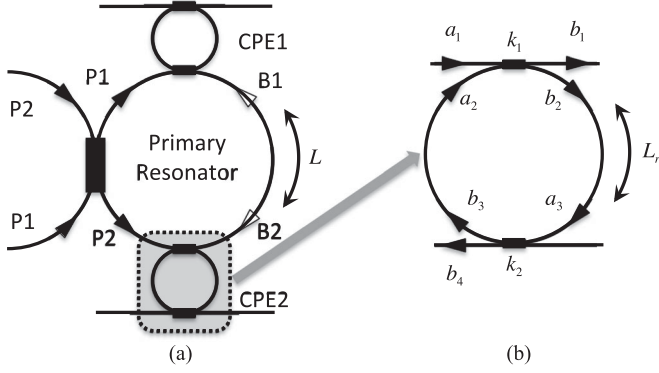


Fig. 1. (a) Schematic illustration of the basic concept of AFLIFOS; (b) Cavity phase element.

anomalous dispersion necessary for the superluminal effect. The details of the scheme will be discussed later in Section III. In this section, we discuss in detail the functionality of each of these auxiliary resonators, focusing on the section in (a) that is enclosed with dashed lines. This section is illustrated in greater detail in Fig. 1(b). In what follows, we will refer to this section as a cavity phase element (CPE).

As illustrated in Fig. 1(b), a CPE consists of a fiber ring resonator coupled to the primary resonator as well as another segment of fiber, and can be used to produce a negative dispersion.  $a_i$  and  $b_i$  are complex amplitudes of the fields. We denote the intensity coupling coefficients as  $k_i$  ( $i = 1, 2$ ) for the two couplers. We assume that each coupler is internally lossless. Using the transfer matrix method, we calculate the effective transmissivity and reflectivity of the CPE as

$$t_{CPE} \equiv \frac{b_1}{a_1} = \frac{\sqrt{1-k_1} - \sqrt{1-k_2} e^{i\phi}}{1 - e^{i\phi} \sqrt{1-k_1} \sqrt{1-k_2}} \equiv |t_{CPE}| e^{i\theta_{CPE}}, \quad (1)$$

$$r_{CPE} \equiv \frac{b_4}{a_1} = \frac{-e^{i\phi/2} \sqrt{k_1} \sqrt{k_2}}{1 - e^{i\phi} \sqrt{1-k_1} \sqrt{1-k_2}}, \quad (2)$$

where  $\phi = n_0 \omega L_r / c$  is the phase shift in the CPE ring,  $n_0$  is the effective index of refraction of the fiber,  $L_r$  is the perimeter of the CPE ring, and  $\theta_{CPE}$  is the net phase shift imparted by the CPE ring. The value of  $\theta_{CPE}$  follows immediately from (1):

$$\theta_{CPE} = \tan^{-1} \left[ -\frac{k_1 \sqrt{1-k_2} \sin(\phi)}{\sqrt{1-k_1}(2-k_2) - \sqrt{1-k_2}(2-k_1) \cos(\phi)} \right], \quad (3)$$

We plot in Fig. 2 the amplitude  $|t_{CPE}|$  and the phase  $\theta_{CPE}$  as a function of detuning,  $\Delta/(2\pi)$ , from the resonant frequency for the CPE, where we can see that the CPE produces an absorption dip and a negative dispersion. At the resonant frequency of the CPE ring, which satisfies the condition that  $\phi = 2\pi l$  (where  $l$  is an integer), we get maximal negative slope of the phase.

As noted above, the AFLIFOS architecture employs two non-degenerate, counter-propagating Brillouin pumps. In Section III, we will consider in detail the behavior of the complete system.

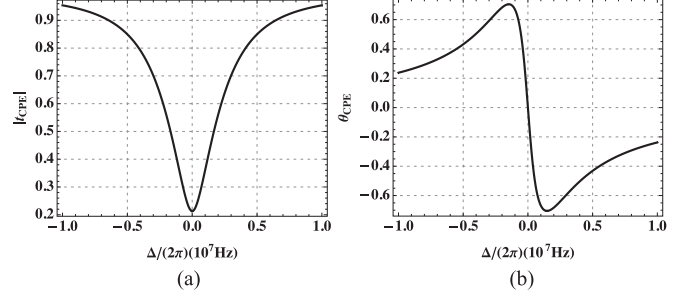


Fig. 2. Plots of (a)  $|t_{CPE}|$  and (b)  $\theta_{CPE}$  as a function of detuning  $\Delta/(2\pi)$  for the CPE.

Here, as an illustration, we consider the case where a single CPE and a single Brillouin pump are present in the system. The resonant frequency of the CPE is set to the peak frequency of the gain. Then the CPE creates an absorption dip in the center of the Brillouin gain, which results in a negative dispersion for the superluminal effect. The width of the Brillouin gain is chosen to be smaller than the resonator free spectral range. Therefore, within the gain peak, there is only one cavity mode. At the edge of the absorption band, lasing is prevented since the phase condition for lasing is not satisfied. The primary resonator has a round-trip length  $L$  [see Fig. 1(a)]. If  $\omega_{res}$  is a frequency that is resonant in the primary resonator, then it follows that

$$\omega_{res} n_0 L / c + \theta_{CPE}(\omega_{res}) + \theta_{Br}(\omega_{res}) = 2\pi K, \quad (4)$$

where  $K$  is an integer, and  $\theta_{Br}$  represents the phase shift from the dispersion induced by the Brillouin pump. The real and imaginary parts of the susceptibility induced by the Brillouin pump can be expressed as:

$$\chi' = \frac{2G(\omega - \omega_0)\Gamma}{2\alpha I + \Gamma^2 + 4(\omega - \omega_0)^2}, \chi'' = \frac{-G\Gamma^2}{2\alpha I + \Gamma^2 + 4(\omega - \omega_0)^2}, \quad (5)$$

where  $G$ ,  $\omega_0$ ,  $\Gamma$ , and  $I$  are, respectively, the gain parameter, the peak frequency of the Brillouin gain, the linewidth (of the Brillouin gain), and the probe intensity per unit area. The parameter  $\alpha$  is such that  $\alpha I$  has the dimension of  $\text{sec}^{-2}$ , and  $\sqrt{\alpha I}$  represents power broadening of the Brillouin gain process. The lasing condition requires that the gain compensates the overall roundtrip losses. We define the quality factor of the primary resonator as  $Q$  in the absence of the Brillouin pump. Then the roundtrip transmissivity of the field amplitude in the cavity is  $t_{cav} = \exp[-kn_0 L / (2Q)]$ . Taking into account the transmissivity  $|t_{CPE}|$  of the CPE, we can write (for gain larger than loss at the onset)

$$t_{cav} |t_{CPE}| \exp[-\chi''(I) n_0 k L / 2] = 1. \quad (6)$$

Solving (6) we can get the value of  $I$  as a function of frequency, from which we can determine  $\theta_{Br}$  after lasing, using  $\theta_{Br} = \chi' k n_0 L / 2$ .

The white light cavity (WLC) condition (which corresponds to maximum superluminal enhancement) requires that the phase accumulated in a round-trip remains  $2\pi K$  regardless of the frequency for a range of frequencies near the resonant frequency

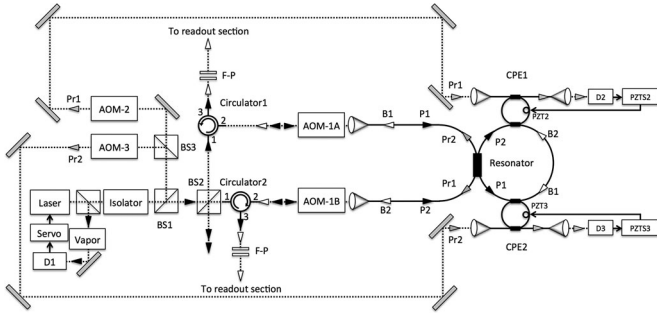


Fig. 3. Schematic diagram of the ring resonator sensor.

of the primary resonator. For a frequency that is  $\Delta\omega$  away from  $\omega_{res}$ , we then have, for the WLC condition:

$$(\omega_{res} + \Delta\omega)n_0L/c + \theta_{CPE}(\omega_{res} + \Delta\omega) + \theta_{Br}(\omega_{res} + \Delta\omega) = 2\pi K, \quad (7)$$

Using the first order approximation in  $\Delta\omega$  that

$$\left. \frac{d\theta}{d\omega} \right|_{\omega_{res}} = \frac{\theta(\omega_{res} + \Delta\omega) - \theta(\omega_{res})}{\Delta\omega}, \quad (8)$$

and using (4) and (7), we get

$$\left. \frac{d\theta}{d\omega} \right|_{\omega_{res}} + \left. \frac{d\theta_{Br}}{d\omega} \right|_{\omega_{res}} = -\frac{n_0}{c}L. \quad (9)$$

We take the resonant frequency  $\omega_{res}$  to be the same as the resonant frequency of the auxiliary resonator in the CPE. For a given set of  $L$ ,  $L_r$ , and  $\omega_{res}$ , the left-hand side of (9) depends on the values of  $k_1$  and  $k_2$ . In our simulation, we fix  $k_1$  as 0.1, and determine  $k_2$  from this equation.

### III. DESCRIPTION OF AFLIFOS

Fig. 3 shows a schematic diagram of the ring resonator sensor embodying the AFLIFOS. The source laser is locked to one of the optical resonances in an acetylene vapor cell using saturated absorption spectroscopy [18]–[20]. For specificity, we consider the laser to be locked to the R(5) line at 1530.24 nm in the  $v_1 + v_3$  bands of  $^{13}\text{C}_2\text{H}_2$ , whose linewidth can be as small as 0.7 kHz [21], [22]. For simplicity in our simulation, we use a wavelength of 1530 nm, rather than 1530.24 nm. This choice does not affect the results for the enhancement factor significantly. The output of the locked laser is passed through an isolator, and split by a beam splitter (BS1) into two equal-powered beams. One of these beams is again split into two equal-powered beams P1 and P2 by another beam splitter (BS2), which are frequency shifted by two separate acoustic-optic modulators (AOM-1A and AOM-1B, respectively) after passing through two separate circulators (Circulator1 and Circulator2, respectively). The resulting beams, P1 and P2, are coupled to the primary fiber ring resonator in opposite directions. The frequencies of AOM-1A and AOM-1B differ by an amount that is  $m$  times the free spectral range of the primary resonator, where  $m \geq 1$  is an integer. Thus, the two laser modes are non-degenerate, which enables determination of the sign of rotation and eliminates the lock-in problem [23], [24]. Two Brillouin lasers, B1 and B2, are produced along directions opposite

to those of the respective pumps. The outputs from port 3 of Circulator1 and Circulator2 are each sent through a Fabry-Perot cavity, which blocks out the pump, and then sent to the readout section. The primary resonator is coupled to cavity phase elements CPE1 and CPE2 in order to produce superluminal effects.

The other beam produced by BS1 is split into two equal-powered beams Pr1 and Pr2 by another beam splitter (BS3). These are frequency shifted by AOM-2 and AOM-3, respectively. Each of these “master” beams (Pr1 and Pr2) is sent to the side fiber in the corresponding CPE and the output from the fiber is detected and used as a feedback signal to stabilize the perimeter of the corresponding CPE with the use of PZTs. Here, for simplicity, we have shown CPE1 and CPE2 to be circular. In practice, the auxiliary cavities are configured in a figure-eight shape in order to eliminate sensitivity of the resonances in these cavities to the Sagnac effect.

The ring resonator system can be used to detect differential mode effects, e.g., a rotation rate  $\Omega$  orthogonal to its plane. Effectively, the rotation of the resonator can be viewed as a change,  $\delta L$ , in the resonator perimeter for B1, and an opposite change  $-\delta L$  for B2 [6]. With these changes in the perimeter  $L$ , the frequency changes for B1 and B2 are, respectively,  $\delta\omega_1$  and  $\delta\omega_2$ , with [25]

$$\delta\omega_2 = \omega\delta L/L = -\delta\omega_1. \quad (10)$$

Therefore, the beat frequency of B1 and B2 is  $\delta\omega_0 = \delta\omega_2 - \delta\omega_1 = 2\omega\delta L/L$ . For rotation sensing, we get, according to the Sagnac effect, that

$$\delta\omega_0 = \frac{\omega}{cn_0} \frac{4\Omega A}{L}, \quad (11)$$

where  $\Omega$  is the rotation rate,  $A$  is the area enclosed by the resonator,  $n_0$  is the index of refraction for the fiber, and  $c$  is the vacuum speed of light. We can thus see that detecting changes in the perimeter of the same magnitude  $\delta L$  but different signs for two counter-propagating lights is equivalent to detecting a rotation rate of

$$\Omega = \frac{cn_0\delta L}{2A}. \quad (12)$$

Besides the application as a gyroscope, this system can also be used as a sensor for detecting the change in the perimeter of the primary ring resonator. This will correspond to sensing common mode effects such as strain.

In this design, two different types of beat signals are to be measured: (a) the beat between the two superluminal lasers, and (b) the beat between each superluminal laser and the master beam to which the corresponding CPE is stabilized. These signals can be processed to determine the differential effects (e.g., rotation) and common mode effects (e.g., strain), the details of which are discussed in Section VI.

### IV. SENSITIVITY ENHANCEMENT

To achieve the optimal condition for sensing, the resonance frequencies of CPE1 and the B1 mode of the primary resonator are both tuned to be at the peak frequency of the Brillouin gain for B1, denoted as  $\omega_{01}$ . Similarly, the resonance frequencies of CPE2 and the B2 mode of the primary resonator are both

tuned to be at the peak frequency of the Brillouin gain for B2, denoted by  $\omega_{02}$ . It should be noted that the resonance condition for each of the two lasing modes (B1 and B2) are affected by both phase elements (CPE1 and CPE2). We consider the case where  $\omega_{01}$  and  $\omega_{02}$  are separated by around 12 times the free spectral range (FSR) of the primary ring resonator. Each pump induces Brillouin absorption (gain) for a counter-propagating probe beam having a frequency that is higher (lower) than that of the pump by the Brillouin frequency shift  $\omega_B = 10.867$  GHz [5]. The WLC condition is then determined by the following set of equations

$$\omega_{01}n_0L/c + \theta_{CPE1}(\omega_{01}) + \theta_{CPE2}(\omega_{01}),$$

$$+ \theta_{Br1}(\omega_{01}) + \theta_{Ab1}(\omega_{01}) = 2\pi M \quad (13)$$

$$(\omega_{01} + \Delta\omega)n_0L/c + \theta_{CPE1}(\omega_{01} + \Delta\omega) + \theta_{CPE2}(\omega_{01} + \Delta\omega),$$

$$+ \theta_{Br1}(\omega_{01} + \Delta\omega) + \theta_{Ab1}(\omega_{01} + \Delta\omega) = 2\pi M \quad (14)$$

$$\omega_{02}n_0L/c + \theta_{CPE1}(\omega_{02}) + \theta_{CPE2}(\omega_{02}),$$

$$+ \theta_{Br2}(\omega_{02}) + \theta_{Ab2}(\omega_{02}) = 2\pi N \quad (15)$$

$$(\omega_{02} + \Delta\omega)n_0L/c + \theta_{CPE1}(\omega_{02} + \Delta\omega) + \theta_{CPE2}(\omega_{02} + \Delta\omega),$$

$$+ \theta_{Br2}(\omega_{02} + \Delta\omega) + \theta_{Ab2}(\omega_{02} + \Delta\omega) = 2\pi N \quad (16)$$

Here  $\theta_{CPE_j}$  is the phase shift from CPE $_j$ , and  $M$  and  $N$  are integers. We have also included the frequency pulling effect by considering the phase terms due to the dispersion from the Brillouin gain ( $\theta_{Br_j}$ ) and absorption ( $\theta_{Ab_j}$ ) induced by the pump P $_j$ . Notice that only the field that is counter-propagating to the Brillouin pump experiences the corresponding Brillouin gain/absorption.

We assume that  $n_0 = 1.45$  is the same for all fiber media, and choose the perimeter of the primary resonator to be  $L = L^{(0)} + \Delta L$ , where  $L^{(0)} = 10.5$  m. To attain resonant pumping and resonant Brillouin lasing simultaneously, we need to choose the value of  $\Delta L$  to be such that while Brillouin lasers (B1 and B2) are on resonance, the pumps P1 and P2 are also close to resonance. The frequency of P1 (P2) is  $\omega_{P1} = \omega_{01} + \omega_B$  ( $\omega_{P2} = \omega_{02} + \omega_B$ ), which is assumed to be  $\Delta\omega_{P1}$  ( $\Delta\omega_{P2}$ ) away from the nearest cavity mode at  $\omega'_{P1}$  ( $\omega'_{P2}$ ). Therefore, we find the following conditions:

$$\omega'_{P1}n_0L/c + \theta_{CPE1}(\omega'_{P1}) + \theta_{CPE2}(\omega'_{P1}),$$

$$+ \theta_{Br2}(\omega'_{P1}) + \theta_{Ab2}(\omega'_{P1}) = 2\pi J_1 \quad (17)$$

$$\omega'_{P2}n_0L/c + \theta_{CPE1}(\omega'_{P2}) + \theta_{CPE2}(\omega'_{P2}),$$

$$+ \theta_{Br1}(\omega'_{P2}) + \theta_{Ab1}(\omega'_{P2}) = 2\pi J_2 \quad (18)$$

where  $\omega'_{P_j} = \omega_{P_j} + \Delta\omega_{P_j}$ ,  $j = 1, 2$ ,  $J_j$  is an integer.

We choose the perimeters of the CPEs to be  $L_{CPE1} = L_{CPE1}^{(0)} + \Delta L_{CPE1}$  and  $L_{CPE2} = L_{CPE2}^{(0)} + \Delta L_{CPE2}$ , where  $L_{CPE1}^{(0)}$  and  $L_{CPE2}^{(0)}$  are each fixed to be 0.78 m. For CPE1, we define  $k_{11}$  and  $k_{21}$  to be the intensity coupling coefficients for the interface with the primary resonator and the external fiber, respectively. The corresponding coefficients for CPE2 are defined as  $k_{12}$  and  $k_{22}$ . With  $k_{11} = k_{12} = 0.1$ , we scan  $\Delta L$ ,  $\Delta L_{CPE1}$ ,  $\Delta L_{CPE2}$ ,  $k_{21}$  and  $k_{22}$  to obtain the optimal operating condition. The optimal values are found to be  $\Delta L \approx 1.14$  cm,

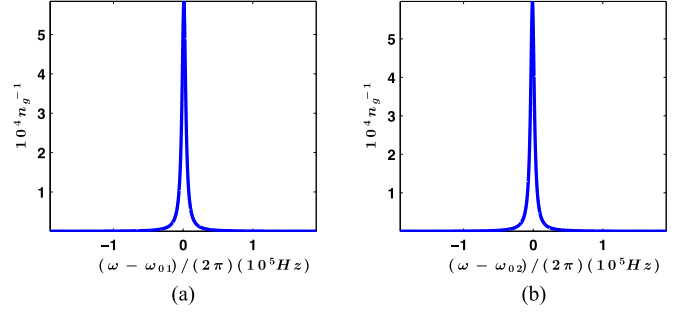


Fig. 4. Plot of the inverse of the group index  $n_g^{-1}$  versus frequency around the center frequency of (a)  $\omega_{01}$  and (b)  $\omega_{02}$ .

$\Delta L_{CPE1} \approx \Delta L_{CPE2} \approx 0.71$  mm, and  $k_{21} \approx k_{22} \approx 0.1501$ . In this case, the frequency difference between the pumps and the nearest resonances are  $\Delta\omega_{P1}/(2\pi) \approx 7.5$  kHz and  $\Delta\omega_{P2}/(2\pi) \approx -7.9$  kHz, which are more than  $\sim 60$  times smaller compared to the linewidth of the primary resonator of 0.46 MHz. The amount of frequency shifts for the various beams are as follows:  $\sim 615.5$  MHz for AOM-1A,  $\sim 850.8$  MHz for AOM-1B,  $\sim 335.3$  MHz for AOM-2, and  $\sim 597.8$  MHz for AOM-3.

The inverse of the group index ( $n_g^{-1}$ ) for optimal operating conditions is plotted in Fig. 4. The peak value at the center reaches as high as  $5.8 \times 10^4$ , which corresponds to the enhancement in sensitivity when the effective change in the perimeter due to common-mode or differential-mode effects is infinitesimal. The enhancement factor is reduced for increasing change in the length of the perimeter, as discussed in more details later.

When the change in the perimeter for B1 is  $\delta L$  while that for B2 is  $-\delta L$ , the round trip (RT) phases for frequencies at  $(\omega_{01} + \delta\omega_{B1})$  and  $(\omega_{02} + \delta\omega_{B2})$ , respectively, are

$$\vartheta_{RT1} = (\omega_{01} + \delta\omega_{B1})n_0(L + \delta L)/c + \theta_{CPE1}(\omega_{01} + \delta\omega_{B1}),$$

$$+ \theta_{CPE2}(\omega_{01} + \delta\omega_{B1}) + \theta_{Br1}(\omega_{01} + \delta\omega_{B1})$$

$$+ \theta_{Ab1}(\omega_{01} + \delta\omega_{B1}), \quad (19)$$

$$\vartheta_{RT2} = (\omega_{02} + \delta\omega_{B2})n_0(L - \delta L)/c + \theta_{CPE1}(\omega_{02} + \delta\omega_{B2}),$$

$$+ \theta_{CPE2}(\omega_{02} + \delta\omega_{B2}) + \theta_{Br2}(\omega_{02} + \delta\omega_{B2})$$

$$+ \theta_{Ab2}(\omega_{02} + \delta\omega_{B2}). \quad (20)$$

We define  $\delta\vartheta_{RT1} \equiv \vartheta_{RT1} - 2\pi M$  and  $\delta\vartheta_{RT2} \equiv \vartheta_{RT2} - 2\pi N$ , where  $M$  and  $N$  are the same as in (13)–(16). The change in the resonant frequency for B1, denoted by  $\delta\omega_{B1}$ , and that for B2, denoted by  $\delta\omega_{B2}$ , are then determined by  $\delta\vartheta_{RT1} = 0$  and  $\delta\vartheta_{RT2} = 0$ .

We plot in Fig. 5 the value of  $\delta\vartheta_{RT1}$  for B1 around  $\omega_{01}$  and  $\delta\vartheta_{RT2}$  for B2 around  $\omega_{02}$  when  $\delta L$  is 0.1 nm. In this case, the enhancement factor for B1 ( $\xi_1 = \delta\omega_{B1}/\delta\omega_1$ ) and that for B2 ( $\xi_2 = \delta\omega_{B2}/\delta\omega_2$ ) are both  $\sim 91$ . For rotation sensing,  $\delta L = 0.1$  nm corresponds to a rotation rate of 1.4 deg/sec, if we consider the primary resonator that consist of ten loops with each loop approximately 1 m in length. Of course, akin to what was done in [17], by adjusting the parameters such as the perimeters and the coupling coefficients, it is possible to

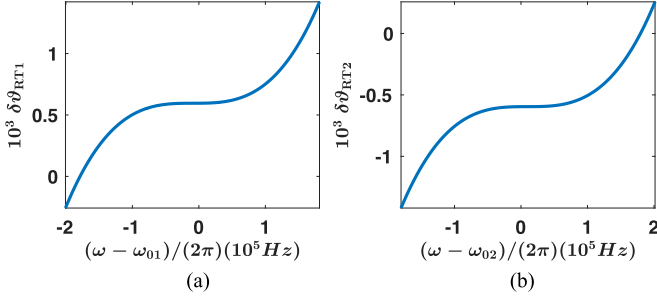


Fig. 5. Plots of (a) the change in the roundtrip phase  $\delta\theta_{RT1}$  versus frequency for B1 around  $\omega_{01}$  and (b)  $\delta\theta_{RT2}$  for B2 around  $\omega_{02}$  with  $\delta L = 0.1$  nm.

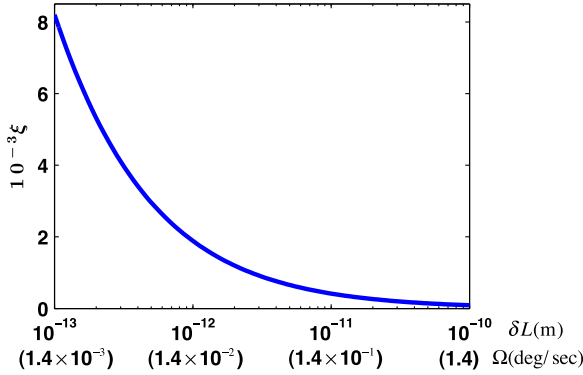


Fig. 6. Plot of the enhancement factor  $\xi$  as a function of the change  $\delta L$  in the length of the primary resonator, or the corresponding rotation rate  $\Omega$ .

get much higher enhancement. We have also investigated the degree of enhancement achievable for different values of  $\delta L$ . This is illustrated in Fig. 6. We show that the enhancement factor  $\xi_1 \cong \xi_2 \equiv \xi$  increases with smaller change in the length of the resonator  $\delta L$ , corresponding to a smaller rotation rate  $\Omega$ . When  $\delta L = 0.1$  pm corresponding to a rotation rate of  $\Omega = 1.4 \times 10^{-3}$  deg/sec, the enhancement factor is  $8.2 \times 10^3$ .

When the system is used for common mode sensing, the changes in the length  $\delta L$  are in the same direction for B1 and B2. The system can be operated in the same condition as in Fig. 5, and the enhancement factor is  $\sim 91$  for both B1 and B2 when  $\delta L = 0.1$  nm.

The minimum measurable spectral uncertainty  $\Delta\omega_{QN}$  for the active ring resonator determines the minimum measurable rotation rate  $\Omega_{MIN}$  [26]–[29], that is,  $\Delta\omega_{QN} = \eta_{ENH,\Omega} \Omega_{MIN}$ , where  $\eta_{ENH,\Omega} \equiv \delta\omega_B/\Omega = \xi\eta_{0,\Omega}$  is the enhanced sensitivity for detecting the rotation rate, and  $\eta_{0,\Omega} \equiv \delta\omega_0/\Omega = 4\omega A/(cn_0L)$  follows from (11). In general, the spectral uncertainty is given by the geometric mean of twice Schawlow-Townes linewidth ( $\gamma_{STL}$ ) for each laser and the measured bandwidth  $\gamma_M = \tau_M^{-1}$ :

$$\Delta\omega_{QN} = \sqrt{2\gamma_{STL}\gamma_M} = \frac{1}{\tau_c} \sqrt{\frac{\hbar\omega_0}{P_{OUT}\tau_M}}, \quad (21)$$

where  $\gamma_c = \tau_c^{-1} = \omega_0/Q$  is the empty cavity decay rate,  $P_{OUT}$  is the output power, and  $\tau_M$  is the measurement time. In Ref. 30, we have shown via numerical simulation that the decay rate of a perturbation in a superluminal laser is close to that

for a conventional laser with identical parameters. As such, it is reasonable to assume that the spectral uncertainty for a superluminal laser will be given by this expression [i.e., (21)]. The minimum measurable rotation rate is then

$$\Omega_{MIN} = \frac{S}{\xi} (P_{OUT}\tau_M)^{-1/2}, S = \frac{cn_0L}{4\omega A} \frac{1}{\tau_c} (\hbar\omega_0)^{1/2}. \quad (22)$$

The value of  $\Omega_{MIN}$  when  $P_{OUT} = 1$  mW and  $\tau_M = 1$  sec is used as a reference, which is  $\Omega_{MIN,REF} = 2.4 \times 10^{-11}$  deg/sec, where the enhancement factor  $\xi \cong 8.2 \times 10^3$  when  $\delta L = 0.1$  pm is used. Therefore, the minimum measurable rotation rate for arbitrary values of  $P_{OUT}$  and  $\tau_M$  is  $\Omega_{MIN} = \Omega_{MIN,REF} (\tilde{P}_{OUT} \cdot \tilde{\tau}_M)^{-1/2}$ , where  $\tilde{P}_{OUT} = P_{OUT}/(1 \text{ mW})$  and  $\tilde{\tau}_M = \tau_M/(1 \text{ sec})$ .

Similarly, we can determine the minimum measurable strain. Since for detection of the common mode effect, a pickoff from the master laser needs to be mixed with the Brillouin laser, the minimum measurable spectral uncertainty is determined by

$$\Delta\omega_{MIN} = \sqrt{(\gamma_{STL} + \gamma_{ML})\gamma_M} \quad (23)$$

where  $\gamma_{ML}$  is the linewidth of the master laser. If the master laser is at the quantum limit,  $\gamma_{ML}$  will be the same as the STL for the master laser. However, that may not be the case for a commercial laser. Thus, we use the best available practical laser, which has  $\gamma_{ML} = 200$  Hz. The STL for the Brillouin laser  $\gamma_{STL} = \hbar\omega_0/(2P_{OUT}\tau_c^2)$  will be larger than 1 kHz when the output power is lower  $4.4 \times 10^{-10}$  W. Since typically the output power is much higher than that, we can ignore the contribution of  $\gamma_{STL}$  in (23).

Suppose that a part of the primary resonator is sensitive to strain, whose length is a fraction  $F$  of the length of the primary resonator  $L$ . The minimum measurable strain [ $h = \delta L/(FL)$ ] is determined by  $\Delta\omega_{MIN} = \eta_{ENH,h} h_{MIN}$ , where  $\eta_{ENH,h} \equiv \delta\omega_B/h = \xi\eta_{0,h}$  is the enhanced sensitivity for strain measurement, and  $\eta_{0,h} \equiv \delta\omega_0/h = \omega_0 F$ . Therefore, the minimum measurable strain is

$$h_{MIN} = \frac{S_h}{\xi F} \sqrt{\frac{\gamma_{ML}}{\tau_M}}, S_h = \frac{1}{\omega_0}, \quad (24)$$

The value of  $h_{MIN}$  when  $F = 1/4$  and  $\gamma_{ML} = 200$  Hz is used as a reference, which is  $h_{MIN,REF} = 1.4 \times 10^{-2} \text{ f}\epsilon/\sqrt{\text{Hz}}$ , which means the minimum measurable change in the length of the primary resonator is  $3.7 \times 10^{-2} \text{ fm}/\sqrt{\text{Hz}}$ . Thus, the minimum measurable strain for arbitrary values of  $F$  and  $\gamma_{ML}$  can be written as  $h_{MIN} = h_{MIN,REF} (\tilde{F}^{-1} \cdot \tilde{\gamma}_{ML}^{1/2})$ , where  $\tilde{F} = 4F$  and  $\tilde{\gamma}_{ML} = \gamma_{ML}/(200 \text{ Hz})$ . Fiber Bragg gratings are often used for building a highly sensitive strain sensor. The lowest value for the minimum measurable strain of a fiber strain sensor is as low as  $30 \text{ f}\epsilon/\sqrt{\text{Hz}}$  with a length of 25 mm [31], [32]. This means a minimum measurable length change of  $0.75 \text{ fm}/\sqrt{\text{Hz}}$ , which is  $\sim 20$  times larger than the value we showed above.

## V. STABILIZATION OF THE CPE LENGTHS

In order to stabilize the perimeter of each CPE, we send a master laser (Pr1/Pr2) to the side fiber in the CPE and detect the output signal using the detectors (D1/D2), as shown in Fig. 3.

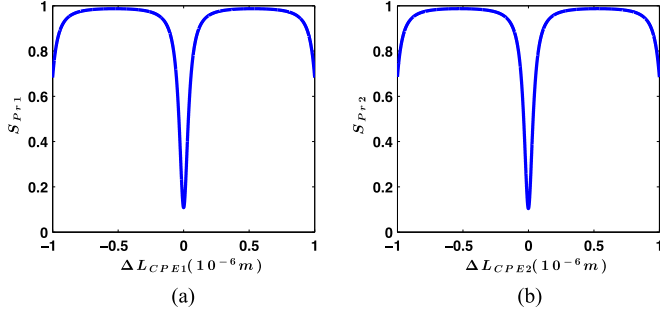


Fig. 7. (a) Plot of the output signal  $S_{Pr1} = |t_{Pr1}|^2$  versus the change  $\Delta L_{CPE1}$  in the perimeter of CPE1; (b) plot of the output signal  $S_{Pr2} = |t_{Pr2}|^2$  versus the change  $\Delta L_{CPE2}$  in the perimeter of CPE2.

The output  $t_{Pr1}$  ( $t_{Pr2}$ ) from the side fiber of Pr1 (Pr2) normalized by the input can be calculated from

$$t_{Pr1} = t'_{CPE1} + \frac{r_{CPE1}^2 t_{CPE2} t_{cav} g_{Br2} g_{Ab2}}{1 - t_{CPE1} t_{CPE2} t_{cav} g_{Br2} g_{Ab2}}, \quad (25)$$

$$t_{Pr2} = t'_{CPE2} + \frac{r_{CPE2}^2 t_{CPE1} t_{cav} g_{Br1} g_{Ab1}}{1 - t_{CPE1} t_{CPE2} t_{cav} g_{Br1} g_{Ab1}}, \quad (26)$$

Here  $t_{CPEj}$  and  $r_{CPEj}$  are the effective transmissivity and reflectivity of CPE $j$  ( $j = 1, 2$ ) following (1) and (2),  $g_{Brj} = |g_{Brj}|e^{i\theta_{Brj}}$  is the Brillouin gain from P $j$ ,  $g_{Abj} = |g_{Abj}|e^{i\theta_{Abj}}$  is the Brillouin absorption from P $j$ , and  $t'_{CPEj}$  is determined by

$$t'_{CPEj} = \frac{\sqrt{1 - k_{2j}} - \sqrt{1 - k_{1j}} e^{i\phi_j}}{1 - e^{i\phi_j} \sqrt{1 - k_{1j}} \sqrt{1 - k_{2j}}}, \quad (27)$$

As the perimeter of the CPE $j$  ( $j = 1, 2$ ) deviates from  $L_{CPEj}$  by an amount of  $\Delta L_{CPEj}$ , the output changes as shown in Fig. 7. Each of the output signals is sent to an AC-Servo, which stabilizes the perimeter of CPE $j$  to the center dip position where  $\Delta L_{CPEj} = 0$  ( $j = 1, 2$ ) as shown in Fig. 7. The frequency modulation necessary for the AC-servo can be applied to AOM-2 and AOM-3.

## VI. SIMULTANEOUS DETECTION OF COMMON-MODE AND DIFFERENTIAL-MODE EFFECTS

In this section, we discuss how to detect, simultaneously, effects due to common-mode and differential-mode perturbations. As specific examples, we consider rotation as a differential mode effect, and strain as a common mode effect. However, the same analysis would also apply to other such effects. In the absence of rotation and strain, we assume the frequency of the CW laser (B1) to be  $f_{B1}$ , and the frequency of the CCW laser (B2) to be  $f_{B2}$ . The corresponding mode numbers are  $m$  and  $(m + 12)$ , respectively. In the case we consider below,  $m$  is around  $1.0 \times 10^7$ .

The common mode effect can be represented as a common change in the length  $\delta L_{COM}$  for both B1 and B2. The frequency change in each Brillouin laser (B1/B2) as a result of the common mode effect is a function of  $\delta L_{COM}$ . Assume that the frequency change is  $F_{COM1}(\delta L_{COM})$  for B1 and  $F_{COM2}(\delta L_{COM})$  for B2. Similarly, the differential mode effect can be represented as a change in the length  $\delta L_{DIF}$  for B1 and  $-\delta L_{DIF}$  for B2. The

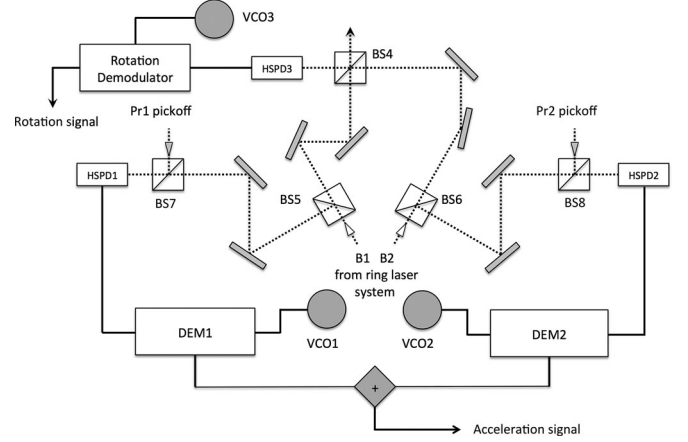


Fig. 8. Schematic illustration of the readout section.

frequency change for each laser due to the differential mode effect is again a function of  $\delta L_{DIF}$ , which is assumed to be  $F_{DIF1}(\delta L_{DIF})$  for B1 and  $-F_{DIF2}(\delta L_{DIF})$  for B2, respectively. Notice that the functions  $F_{COM,j}$  and  $F_{DIF,j}$  ( $j = 1, 2$ ) have odd symmetries. In the presence of possible rotation and strain, represented by  $\delta L_{COM}$  and  $\delta L_{DIF}$ , we can express the lasing frequencies as

$$f'_{B1} = f_{B1} + F_{COM1}(\delta L_{COM}) + F_{DIF1}(\delta L_{DIF}) \quad (28)$$

$$f'_{B2} = f_{B2} + F_{COM2}(\delta L_{COM}) - F_{DIF2}(\delta L_{DIF}) \quad (29)$$

Since the mode number  $m$  is very large ( $2 \times 10^7$ ), the common-mode-effect induced frequency shifts have almost the same magnitudes in each direction, even though the base frequencies differ by 12 times the FSR. The same approximation also applies for the differential-mode-effect induced frequency shifts. We can then simplify the analysis by assuming  $F_{COM1}(\delta L_{COM}) \cong F_{COM2}(\delta L_{COM}) \equiv F_{COM}(\delta L_{COM})$  and  $F_{DIF1}(\delta L_{DIF}) \cong F_{DIF2}(\delta L_{DIF}) \equiv F_{DIF}(\delta L_{DIF})$ .

The readout process (see Fig. 8) measures the frequency differences induced in the two Brillouin lasers in order to extract the rotation and strain experienced by the system. There are four signals that are used in this process: the two Brillouin laser outputs (B1 and B2), and the pickoffs from the master lasers (Pr1 and Pr2).

The two superluminal lasers, B1 and B2, are combined with each other on a 50/50 beamsplitter (BS4) and its output is directed into a high-speed photodetector (HSPD3). The beat frequency at HSPD3 will be  $f_{B2} - f_{B1} - 2F_{DIF}(\delta L_{DIF})$ , which is less (greater) than the frequency difference between the two superluminal lasers expected from an undisturbed system ( $f_{B2} - f_{B1} \equiv \Delta f$ ) if  $F_{DIF}(\delta L_{DIF})$  is positive (negative). The beatnote measured by this detector is then mixed with the output of a voltage controlled oscillator (VCO3) set to match  $\Delta f$  and is demodulated using the rotation demodulator, which is a phase-locked-loop frequency demodulator (PLL-FD) [33]. As a result, we get a signal of  $F_{DIF-DET} = |2F_{DIF}(\delta L_{DIF})|$ . This gives the magnitude of rotation, but not direction [i.e., it does not reveal the sign of  $F_{DIF}(\delta L_{DIF})$ ]. However, we

can remedy this easily as follows. We modulate the frequency of VCO3 around its quiescent value of  $\Delta f$ . When the VCO3 frequency is  $\Delta f + |\varepsilon|$ ,  $F_{DIF-DET}$  will be greater than  $|2F_{DIF}(\delta L_{DIF})|$  if the sign of  $F_{DIF}(\delta L_{DIF})$  is positive, and less than  $|2F_{DIF}(\delta L_{DIF})|$  if the sign of  $F_{DIF}(\delta L_{DIF})$  is negative. Thus, we can determine both magnitude and sign of  $F_{DIF}(\delta L_{DIF})$ . Alternatively, we can determine the sign of  $F_{DIF}(\delta L_{DIF})$  by sending a small part of the output from HSPD3 through a low-pass filter (LPF) whose maximal slope is set to  $\Delta f$  and then detecting the power of the filtered signal. We calibrate the LPF with the output power  $P_{LPF}$  of the signal when the system is undisturbed. In a disturbed system, if the output power is lower than  $P_{LPF}$ , the sign of  $F_{DIF}(\delta L_{DIF})$  is negative; otherwise, the sign of  $F_{DIF}(\delta L_{DIF})$  is positive.

To determine the common mode effect, a small part of each Brillouin laser is combined with its corresponding master laser on a 50/50 beamsplitter (BS7/BS8) and the resulting beat signal is detected with a high-speed photodetector (HSPD1/HSPD2). The output of each detector is then mixed with the output of a voltage-controlled oscillator (VCO1/VCO2) set at  $f_1/f_2$ , which equals the difference in frequency between the master laser and the Brillouin laser from the undisturbed system. This signal is sent to a low pass filter so that we get only the difference frequency and then it is converted to a voltage signal using a PLL-FD (DEM1/DEM2). As a result, we get a DC signal proportional to the departure of each superluminal laser frequency from the value expected from an unmoving system.

Consider now the output of DEM1. It will produce a signal proportional to  $|F_{COM}(\delta L_{COM}) + F_{DIF}(\delta L_{DIF})|$ . By modulating VCO1 around  $f_1$ , we can determine the magnitude as well as the sign of the signal produced by beating the output of HSPD1 with VCO1. For example, by increasing the frequency of VCO1 slightly, if we see an increase in the output, we can determine that  $\delta f_1 = F_{COM}(\delta L_{COM}) + F_{DIF}(\delta L_{DIF}) > 0$ ; otherwise, if we see a decrease in the output, we can determine that  $\delta f_1 < 0$ . Alternatively, we can determine the sign of  $\delta f_1$  using a low pass filter whose maximum slope is set to the frequency difference between the master laser and the Brillouin laser, similarly to the process described in the differential-mode detection. Thus, we can produce a voltage that corresponds to  $\delta f_1 = F_{COM}(\delta L_{COM}) + F_{DIF}(\delta L_{DIF})$  rather than  $|\delta f_1|$ . Similarly, by modulating VCO2 around  $f_2$ , we can produce a voltage that corresponds to  $\delta f_2 = F_{COM}(\delta L_{COM}) - F_{DIF}(\delta L_{DIF})$  rather than  $|\delta f_2|$ . Summing up these two signals yields  $2F_{COM}(\delta L_{COM})$ , from which we can determine the magnitude and sign of  $F_{COM}(\delta L_{COM})$ .

If the difference in mode number  $m$  for B1 mode and  $m + \Delta m$  for B2 mode is taken into account [25], the frequency change due to the common or differential mode effect is different for the two modes, i.e.,  $F_{\alpha 1}(\delta L_{\alpha})/F_{\alpha 2}(\delta L_{\alpha}) = m/(m + \Delta m)$ ,  $\alpha = COM, DIF$ . Note that the output of DEM1 will be a signal proportional to  $|F_{COM1}(\delta L_{COM}) + F_{DIF1}(\delta L_{DIF})|$ . Using the same method as above, we can determine the magnitude as well as the sign of the signal, i.e., we can determine  $\delta f_1 = F_{COM1}(\delta L_{COM}) + F_{DIF1}(\delta L_{DIF})$ . Similarly, we can produce a voltage that corresponds to  $\delta f_2 = F_{COM2}(\delta L_{COM}) - F_{DIF2}(\delta L_{DIF})$ . Therefore, the common mode effect signal can

be produced by

$$F_{COM1}(\delta L_{COM}) = \frac{1}{2}\delta f_1 + \frac{1}{2} \frac{m}{m + \Delta m} \delta f_2, \quad (30)$$

and the differential mode effect signal can be produced by

$$F_{DIF1}(\delta L_{DIF}) = \frac{1}{2}\delta f_1 - \frac{1}{2} \frac{m}{m + \Delta m} \delta f_2. \quad (31)$$

Similarly, if  $F_{COM1}(\delta L_{COM}) \neq F_{COM2}(\delta L_{COM})$  or  $F_{DIF1}(\delta L_{DIF}) \neq F_{DIF2}(\delta L_{DIF})$  due to other reasons and we know their relation, for example, from experiment, it is possible to account for the difference exactly as well.

In proposing the concept presented in this paper, we have used an inherent assumption that, before the superluminal effect is added, the base-line gyroscope is at the quantum noise limit. When this is not true, special care has to be taken to consider the nature of the excess noise and how it may be affected by the superluminal operation. Consider first the case of Rayleigh scattering. It is indeed true that the sensitivity of a typical fiber optic gyroscope may be limited by this scattering. In Ref. 34, it has been pointed out that the error is due primarily to backscattering from one direction to the other, and forward scattering does not add any significant error. In the design proposed here, we are making use of non-degenerate modes in the two directions. As such, the effect of Rayleigh back-scattering should be fully suppressed. On the other hand, the noise due to the Kerr effect [35] is caused by residual imbalance in the power in the two directions. There are schemes [36], [37] that can reduce such errors very significantly. In this paper, we assume that the Kerr effect is suppressed to be below the quantum noise.

## VII. CONCLUSION

We have developed an Active Fast Light Fiber Optic Sensor (AFLIFOS) that can be used for high sensitivity measurements of many parameters of interest, both due to common mode effect (e.g., strain) and differential mode effect (e.g., rotation). Both common mode effects and differential mode effects can be viewed as a change in the length of the primary resonator. The superluminal effects for two counter-propagating Brillouin laser modes are produced by two auxiliary resonators (CPEs) that are coupled to the primary resonator.

We first developed a detailed theoretical model for optimizing the design of the AFLIFOS. In the optimal operating condition, we determined the enhancement factor of the sensitivity for detecting varying magnitude of the change in the length of the primary resonator, corresponding to detecting varying rotation rates, and showed that the factor is  $\sim 8.2 \times 10^3$  under the optimized condition, when the effective change in the length of the primary fiber resonator is 0.1 pm, corresponding to a rotation rate of  $1.4 \times 10^{-3}$  deg/sec. With this enhancement factor, we show that the minimum detectable rotation rate is  $2.4 \times 10^{-11}$  deg/sec when the output power is 1 mW and the measurement time is 1 sec, which is  $\sim 8.2 \times 10^3$  times better than that of the passive version with the same parameters. The minimum measurable strain is  $1.4 \times 10^{-2}$   $f\varepsilon/\sqrt{\text{Hz}}$  when 1/4 of the primary resonator is sensitive to strain and the linewidth of the master laser is taken to be 1 kHz. The minimum

measurable length change is then  $3.7 \times 10^{-2}$  fm/ $\sqrt{\text{Hz}}$ , which is  $\sim 20$  times smaller than that for the fiber strain sensor with the lowest reported minimum measurable strain  $30 \text{ f}\epsilon/\sqrt{\text{Hz}}$  with a length of 25 mm. By adjusting the parameters such as the perimeters and the coupling coefficients, it may be possible to get much higher enhancement. We then showed the design of using master lasers for stabilizing the perimeter of the CPEs. We also showed the design for the readout section, where the beats between two Brillouin lasers and the two reference master lasers are measured. Assuming that the change in frequency for the lasers as a function of the change in the perimeter of the primary resonator is known, we can determine the common mode effects and differential mode effect separately.

In the future, we will carry out experimental demonstration of the AFLIFOS capable of measuring rotation as well as strain. In general, gyroscopes require temperature controls. The main fiber loop and the auxiliary loops will be contained in a foam box to reduce the airflow and hence the temperature variations during the operation of the system. Moreover, for the AFLIFOS we need to use active temperature controller to the precision of 1 mK, because, as recently found in Ref. 38, Brillouin fiber lasers are strongly affected by thermal effects from the change in lasing power. In addition, the whole system is mounted on a floating table to reduce the effect of vibrations. This will make it easier to isolate the Brillouin effect from parasite effects.

## REFERENCES

- [1] M. Terrel, M. Dignonnet, and S. Fan, "Coupled resonator gyroscopes: What works and what does not," *Proc. SPIE*, vol. 7612, 2010, Art. no. 76120B.
- [2] D. D. Smith and H. Chang, "Coherence phenomena in coupled optical resonators," *J. Mod. Opt.*, vol. 51, no. 16–18, pp. 2503–2513, 2004.
- [3] H. Chang and D. D. Smith, "Gain-assisted superluminal propagation in coupled optical resonators," *J. Opt. Soc. Amer. B*, vol. 22, no. 10, pp. 2237–2241, 2005.
- [4] M. Salit, G. S. Pati, K. Salit, and M. S. Shahriar, "Fast-light for astrophysics: Super-sensitive gyroscopes and gravitational wave detectors," *J. Mod. Phys.*, vol. 54, no. 16/17, pp. 2425–2440, 2007.
- [5] G. S. Pati, M. Messall, K. Salit, and M. S. Shahriar, "Demonstration of a tunable-bandwidth white light interferometer using anomalous dispersion in atomic vapor," *Phys. Rev. Lett.*, vol. 99, 2007, Art. no. 133601.
- [6] M. S. Shahriar, G. S. Pati, R. Tripathi, V. Gopal, M. Messall, and K. Salit, "Ultra-high enhancement in absolute and relative rotation sensing using fast and slow light," *Phys. Rev. A*, vol. 75, 2007, Art. no. 53807.
- [7] M. S. Shahriar and M. Salit, "Application of fast light in gravitational wave detection with interferometers and resonators," *J. Mod. Opt.*, vol. 55, no. 19/20, pp. 3133–3147, Nov. 2008.
- [8] G. S. Pati, M. Salit, K. Salit, and M. S. Shahriar, "Demonstration of displacement–measurement–sensitivity proportional to inverse group index of intra-cavity medium in a ring resonator," *Opt. Commun.*, vol. 281, no. 19, pp. 4931–4935, 2008.
- [9] D. D. Smith, H. Chang, L. Arissian, and J. C. Diels, "Dispersion-enhanced laser gyroscope," *Phys. Rev. A*, vol. 78, 2008, Art. no. 053824.
- [10] G. S. Pati, M. Salit, K. Salit, and M. S. Shahriar, "Simultaneous slow and fast light effects using probe gain and pump depletion via Raman gain in atomic vapor," *Opt. Express*, vol. 17, pp. 8775–8780, 2009.
- [11] D. D. Smith, K. Myneni, J. A. Odutola, and J. C. Diels, "Enhanced sensitivity of a passive optical cavity by an intracavity dispersive medium," *Phys. Rev. A*, vol. 80, 2009, Art. no. 011809(R).
- [12] H. N. Yum, M. Salit, J. Yablon, K. Salit, Y. Wang, and M. S. Shahriar, "Superluminal ring laser for hypersensitive sensing," *Opt. Express*, vol. 18, no. 17, pp. 17658–17665, 2010.
- [13] D. D. Smith, H. Chang, K. Myneni, and A. T. Rosenberger, "Fast-light enhancement of an optical cavity by polarization mode coupling," *Phys. Rev. A*, vol. 89, 2014, Art. no. 053804.
- [14] K. Myneni, D. D. Smith, H. Chang, and H. A. Luckay, "Temperature sensitivity of the cavity scale factor enhancement for a Gaussian absorption resonance," *Phys. Rev. A*, vol. 92, 2015, Art. no. 053845.
- [15] D. D. Smith, H. A. Luckay, H. Chang, and K. Myneni, "Quantum-noise-limited sensitivity-enhancement of a passive optical cavity by a fast-light medium," *Phys. Rev. A*, vol. 94, 2016, Art. no. 023828.
- [16] H. N. Yum and M. S. Shahriar, "Pump-probe model for the Kramers-Kronig relations in a laser," *J. Opt.*, vol. 12, 2010, Art. no. 104018.
- [17] O. Kotlicki, J. Scheuer, and M. S. Shahriar, "Theoretical study on Brillouin fiber laser sensor based on white light cavity," *Opt. Express*, vol. 20, no. 27, pp. 28234–28248, 2012.
- [18] M. De Labacherie, K. Nakagawa, and M. Ohtsu, "Ultraviolet  $^{13}\text{C}_2\text{H}_2$  saturated-absorption lines at  $1.5 \mu\text{m}$ ," *Opt. Lett.*, vol. 19, no. 11, pp. 840–842, 1994.
- [19] K. Knabe, "Using saturated absorption spectroscopy on acetylene-filled hollow-core fibers for absolute frequency measurements," Ph.D. dissertation, Kansas State University, Manhattan, KS, USA, 2003.
- [20] R. Thapa, K. Knabe, M. Faheem, A. Naweid, O. L. Weaver, and K. L. Corwin, "Saturated absorption spectroscopy of acetylene gas inside large-core photonic bandgap fiber," *Opt. Lett.*, vol. 31, no. 16, pp. 2489–2491, 2006.
- [21] C. S. Edwards, H. S. Margolis, G. P. Barwood, S. N. Lea, P. Gill, and W. R. C. Rowley, "High-accuracy frequency atlas of  $^{13}\text{C}_2\text{H}_2$  in the  $1.5 \mu\text{m}$  region," *Appl. Phys. B*, vol. 80, pp. 977–983, 2005.
- [22] J. Jiang, A. Onae, H. Matsumoto, and F. L. Hong, "Frequency measurement of acetylene-stabilized lasers using a femtosecond optical comb without carrier-envelope offset frequency control," *Opt. Express*, vol. 13, pp. 1958–1965, 2005.
- [23] W. W. Chow, J. Gea-Banacloche, L. M. Pedrotti, V. E. Sanders, W. Schleich, and M. O. Scully, "The ring laser gyro," *Rev. Mod. Phys.*, vol. 57, no. 1, 1985, Art. no. 61.
- [24] F. Zarinetchi, S. P. Smith, and S. Ezekiel, "Stimulated Brillouin fiber-optic laser gyroscope," *Opt. Lett.*, vol. 16, no. 4, pp. 229–231, 1991.
- [25] If the two laser modes are degenerate ( $\omega_2 = \omega_1 = \omega$ ), we have  $\delta\omega_2 = -\delta\omega_1 = \omega\delta L/L$ . In the non-degenerate case where B1 is in  $m$  mode and B2 is in  $m + \Delta m$  mode, it can be shown that  $-\delta\omega_2/\delta\omega_1 = \omega_2/\omega_1 = (m + \Delta m)/m$ . For  $m \gg \Delta m \geq 1$ , the ratio is approximately one.
- [26] C. H. Townes, "Some applications of optical and infrared masers," in *Advances in Quantum Electronics*, J. R. Singer, Ed. New York, NY, USA: Columbia Univ. Press, 1961, pp. 1–11.
- [27] M. S. Shahriar, G. S. Pati, R. Tripathi, V. Gopal, and M. Messall, "Ultra-high precision rotation sensing using a fast-light enhanced RLG," *Phys. Rev. A*, vol. 75, 2007, Art. no. 053807.
- [28] T. A. Dorschner, H. A. Haus, M. Holz, I. W. Smith, and H. Statz, "Laser gyro at quantum limit," *IEEE J. Quantum. Electron.*, vol. QE-16, no. 12, pp. 1376–1379, Dec. 1980.
- [29] B. T. King, "Application of superresolution techniques to RLGs: Exploring the quantum limit," *Appl. Opt.*, vol. 39, 2000, Art. no. 6151.
- [30] J. Scheuer and S. M. Shahriar, "Lasing dynamics of super and sub luminal lasers," *Opt. Express*, vol. 23, 2015, Art. no. 032350.
- [31] G. Skoliano, A. Arora, M. Bernier, and M. Dignonnet, "Slow light in fiber Bragg gratings and its applications," *J. Phys. D, Appl. Phys.*, vol. 49, 2016, Art. no. 463001.
- [32] G. Skolianos, A. Arora, M. Bernier, and M. Dignonnet, "Measuring attostains in a slow-light fiber Bragg grating," *Proc. SPIE 9763*, 976317, Mar. 2016.
- [33] [Online]. Available: <http://www.radio-electronics.com/info/rf-technology-design/fm-reception/fm-pll-detector-demodulator-demodulation.php>
- [34] C. C. Cutler, S. A. Newton, and H. J. Shaw, "Limitation of rotation sensing by scattering," *Opt. Lett.*, vol. 5, no. 11, pp. 488–490, 1990.
- [35] R. W. Hellwarth, "Theory of phase-conjugation by four-wave mixing in a waveguide," *IEEE J. Quantum Electron.*, vol. QE-15, no. 2, pp. 101–109, Feb. 1979.
- [36] K. Takiguchi and K. Hotate, "Method to reduce the optical Kerr-effect-induced bias in an optical passive ring-resonator gyro," *IEEE Photon. Technol. Lett.*, vol. 4, no. 2, pp. 203–206, Feb. 1992.
- [37] Z. Luo, X. Yuan, Z. Zhu, K. Liu, W. Ye, C. Zeng, and J. Ji, "Brillouin/Raman compensation of the Kerr-effect-induced bias in a nonlinear ring laser gyroscope," *Opt. Lett.*, vol. 38, no. 7, pp. 1152–1154, 2013.
- [38] O. Kotlicki and J. Scheuer, "Lasing frequency self-stabilization in Brillouin Fiber Lasers," in *Proc. Int. Conf. Lasers Electro-Opt.*, 2016, Paper SWIP.6.

Authors' photographs and biographies not available at the time of publication.